

Nonvolatile spin field effect transistor based on $\text{VSi}_2\text{N}_4/\text{Sc}_2\text{CO}_2$ multiferroic heterostructure

Xian Zhang,¹ Bang Liu,² Junsheng Huang,² Xinwei Cao,¹ Yunzhe Zhang,¹ and Zhi-Xin Guo^{2,*}

¹*College of Mechanical and Materials Engineering, Xi'an University, Xi'an 710065, China*

²*State Key Laboratory for Mechanical Behavior of Materials and School of Materials Science and Engineering, Xi'an Jiaotong University, Xi'an, Shaanxi, 710049, China*

(Dated: April 15, 2024)

In this study, we present first-principles calculations that introduce a novel nonvolatile spin field-effect transistor (Spin-FET) utilizing a van der Waals multiferroic heterostructure, specifically $\text{VSi}_2\text{N}_4/\text{Sc}_2\text{CO}_2$. We demonstrate that inverting the ferroelectric polarization in a Sc_2CO_2 monolayer can effectively modulate the electronic states of a VSi_2N_4 monolayer, enabling a transition from half-metal to half-semiconductor. This transition significantly alters the electronic transport properties. Furthermore, we construct a Spin-FET device based on this multiferroic heterostructure and observe that the $\text{VSi}_2\text{N}_4/\text{Sc}_2\text{CO}_2$ -based Spin-FET exhibits exceptional all-electric-controlled performance. Notably, the inversion of the Sc_2CO_2 ferroelectric polarization yields a substantial on-off current ratio, approximately 650%, under a minimal bias voltage of 0.02 V. Additionally, we identify a unique spatially-separated spin-polarized transport phenomenon, wherein pure spin-up electrons transport exclusively through VSi_2N_4 , and spin-down electrons through Sc_2CO_2 . Our findings suggest a promising pathway for developing low-energy-dissipation and nonvolatile FET devices.

I. INTRODUCTION

During the continuous miniaturization of electronic products, Joule heating and quantum limit on devices become the bottlenecks that prevent increases in operation speed and information density, which invalidate the Moore's law^{1,2}. Spintronics is believed to be the strong candidate of the future technology in the post-Si-era³⁻⁸. For any operation in spintronics, the techniques for injection, detection, manipulation, transport, and storage of spins need to be established⁹. In spin-based devices, encoding and reading out spin information in single spins can be considered the ultimate limit for scaling magnetic information. Spin field-effect transistor (Spin-FET) is a fundamental spin-based device for the spin operation^{10,11}. Developing low-power cost Spin-FET that can efficiently realize the *on* or *off* state of pure spin current is crucial for the development of spintronics¹².

Traditionally, Spin-FET is a three terminal device with spin polarized current flowing between drain and source terminals and the gate terminal is used to control this current. As proposed by Datta and Das, the spin precession motion of electron can be controlled through the Rashba spin-orbit coupling effect, where *on* and *off* states are distinguished by π phase difference in spin precession motion^{10,11}. Nonetheless, since the realization of π phase difference in a Spin-FET depends on the precise control of gate voltage, traditional Spin-FETs meet challenge of the nonvolatile functionality, which is usually realized by using a ferroelectric material as gating.

In this work, based on the first-principles calculations, we propose a Spin-FET possessing remarkable nonvolatile *on* and *off* functionality. Such Spin-FET uses a two-dimensional (2D) van der Waals (vdW) multiferroic heterostructure (e.g. composed by mono-

layer VSi_2N_4 and monolayer Sc_2CO_2) as the channel material, instead of the nonmagnetic semiconductors (like InAs, InAlAs, etc.) that are generally adopted in traditional Spin-FETs¹³. In the multiferroic heterostructure, ferromagnetic material VSi_2N_4 has a half-semiconductor characteristic and is mainly responsible for the spin transport^{15,16}. Whereas, the ferroelectric material Sc_2CO_2 has a semiconductor characteristic^{17,18} and is mainly in charge of controlling the spin-polarized electronic structure of VSi_2N_4 .

It is noteworthy that constructing vdW multiferroics with 2D ferroelectrics and ferromagnets and studying their full-electric-control of nonvolatile device applications had been recently explored. Nonetheless, these studies are mostly on the stage of proving a proof-of-concept of all-electric-controlled valving effects^{18,19} accompanied by some pioneer works on the magnetic tunnel junction (MTJ) device applications²⁰⁻²². The concept of using 2D multiferroic heterostructure to realize the nonvolatile Spin-FETs is first proposed here. Moreover, the all-electric-controlled nonvolatile half-semiconducting to half-metallic transition is still to be realized in 2D ferroelectrics.

We find that the inversion of ferroelectric polarization of Sc_2CO_2 can efficiently change the spin-up electronic structure of VSi_2N_4 , leading to a half-semiconductor to half-metal transition. Moreover, the $\text{VSi}_2\text{N}_4/\text{Sc}_2\text{CO}_2$ based Spin-FET has remarkable all-electric-controlled performance, where a large on-off current ratio can be obtained under a small bias voltage. Additionally, an interesting spatially-separated spin-polarized transport phenomenon, i.e., pure spin-up (spin-down) current transporting in VSi_2N_4 (Sc_2CO_2), is observed.

II. METHOD

Geometric optimization and electronic structures of the heterostructure are calculated by density-functional theory (DFT) with the projector-augmented-wave (PAW) method, which is implemented in the Vienna ab initio simulation package^{23,24}. The exchange-correlation interaction is treated by the generalized gradient approximation (GGA) based on the Perdew-Burke-Ernzerhof (PBE) function and HSE06 functional for the geometric optimization and electronic structures, respectively^{25,26}. The convergence standards of the atomic energy and positions are less than 1×10^{-5} eV per atom and 1×10^{-2} eV \AA^{-1} , respectively. The cutoff energy of wave function is set to 500 eV. The Brillouin zone (BZ) is sampled by a $9 \times 9 \times 1$ Monkhorst-Pack k-point mesh.

The transport properties are simulated based on the DFT method combined with the nonequilibrium Green's function (NEGF) formalism, using the Atomistix ToolKit (ATK) 2019 package²⁷. In the calculations, the Tier 3 basis set of the linear combination of atomic orbital (LCAO) is adopted with Hartwigsen-Goedecker-Hutter pseudopotentials and GGA in the form of the PBE function is utilized to represent the exchange and correlation interactions. The transmission calculations are carried out with the PBE pseudopotentials distributed in the QuantumWise package^{27,28}. A density mesh-cutoff of 75 Hartree is employed, and the BZ is sampled using a $6 \times 1 \times 94$ k-point grid in the transport calculations. At a bias-voltage V_b , the spin-resolved current (I_σ) can be calculated as follows:

$$I_\sigma(V_b) = \frac{e}{h} \int_{-\infty}^{+\infty} dE [f(E, \mu_L) - f(E, \mu_R)] T_\sigma(E, V_b), \quad (1)$$

where $f(E, \mu_L)$ and $f(E, \mu_R)$ are the Fermi-Dirac distribution of the left and right electrodes, respectively. μ_L and μ_R are the electrochemical potentials of the left and right electrodes, respectively, and $T_\sigma(E)$ is the transmission probability for an electron at energy E with spin σ . Note that the linear response current originated from the equilibrium transmission spectrum at zero bias is considered in the calculations²⁹.

III. RESULTS

The heterostructure is constructed by a ferromagnetic (FM) monolayer VSi_2N_4 and a ferroelectric monolayer Sc_2CO_2 . The monolayer Sc_2CO_2 was predicted to have a sizable out-of-plane electrical polarization as high as $1.60 \mu\text{C}/\text{cm}^2$, and the reverse of electric polarization is achieved via displacement of C atoms with an energy barrier about 0.52 eV ¹⁷. The Sc_2CO_2 with carbon-up and carbon-down configurations correspond to the polarization-up ($\text{P}\uparrow$) and polarization-down states ($\text{P}\downarrow$), respectively (see Fig. 1(a)). On the other hand, VSi_2N_4

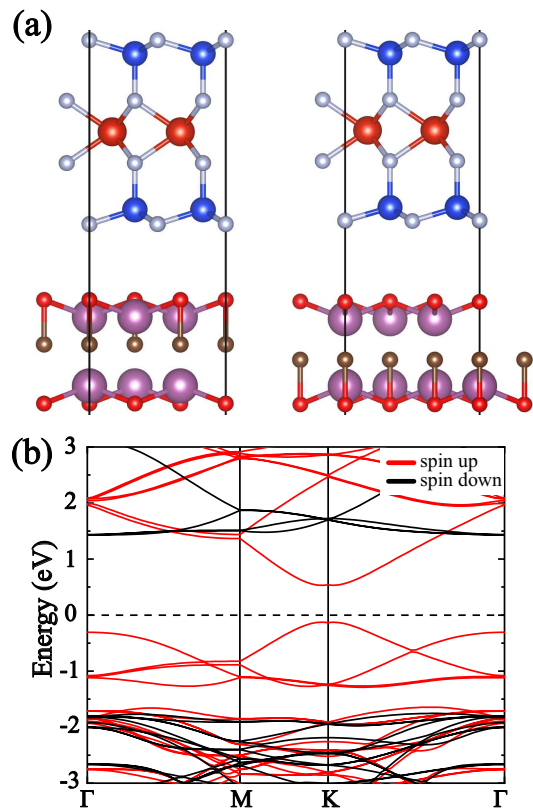


FIG. 1. Atomic structures of $\text{VSi}_2\text{N}_4/\text{Sc}_2\text{CO}_2$ heterostructure with Sc_2CO_2 in $\text{P}\uparrow$ and $\text{P}\downarrow$ polarizations and the spin-resolved energy bands of VSi_2N_4 . (a) Atomic structures of $\text{VSi}_2\text{N}_4/\text{Sc}_2\text{CO}_2$ heterostructure, with Sc_2CO_2 in $\text{P}\uparrow$ (left panel) polarization and $\text{P}\downarrow$ (right panel) polarizations, respectively. (b) Band structure of VSi_2N_4 . The grey, large red, and blue balls represent the N, Si, and V atoms, respectively. The red, big purple, and orange balls represent the O, Sc, and C atoms, respectively.

is a theoretically predicted 2D magnetic material, which is a member of the MA_2Z_4 family. The Curie temperature of monolayer VSi_2N_4 is predicted to be higher than room temperature, showing the promising potential applications in future spintronic devices^{14,15}. Fig. 1(b) further shows the calculated band structure of monolayer VSi_2N_4 . An interesting characteristic is that there is only spin-up electrons in a wide energy range around the Fermi energy (E_F), i.e., $[-1.7, 1.4] \text{ eV}$, making VSi_2N_4 an ideal half-semiconductor.

Considering that the in-plane lattice constant of free-standing Sc_2CO_2 and VSi_2N_4 are 5.74 \AA and 2.88 \AA , respectively, a 2×2 super-periodicity of VSi_2N_4 is commensurate to the 1×1 Sc_2CO_2 , with a lattice mismatch of 1.23%. As shown in Fig. S1, we have considered three typical stacking configurations of the $\text{VSi}_2\text{N}_4/\text{Sc}_2\text{CO}_2$ heterostructure, namely, hollow configuration, bridge configuration, and top configuration. The calculated total energies of the three configurations are -300776.98 meV , -300776.90 meV , and -300776.88 meV ,

respectively, showing that the hollow configuration (also see Fig. 1(a)) is the most stable configuration. Nevertheless, the total energy difference among different configurations is very small (≤ 0.1 meV), indicating that all the three configurations can be obtained in experiments. The interlayer spacings between VSi_2N_4 and Sc_2CO_2 are 2.82 Å and 3.06 Å for the $\text{P}\uparrow$ and $\text{P}\downarrow$ polarization states, respectively. It is known that the atomic radii of O and N atoms, which are located at the surface of Sc_2CO_2 and VSi_2N_4 , respectively, are 0.66 Å and 0.71 Å. Hence, the sum of their atomic radii is much smaller than the interlayer spacing, showing the nature of vdW interaction between Sc_2CO_2 and VSi_2N_4 . To ensure that the $\text{VSi}_2\text{N}_4/\text{Sc}_2\text{CO}_2$ heterostructure is energetically stable, we further calculate the binding energy (E_b) between VSi_2N_4 and Sc_2CO_2 , which is defined as $E_b = (E_S + E_V - E_{tot})/S$. Here E_S , E_V , and E_{tot} are the total energy of monolayer Sc_2CO_2 , monolayer VSi_2N_4 , and $\text{VSi}_2\text{N}_4/\text{Sc}_2\text{CO}_2$ heterostructure, respectively. S represents the interface area of the simulated cell. In the hollow configuration, it is found that $E_b = -31$ meV/Å² and -21 meV/Å² for the $\text{P}\uparrow$ and $\text{P}\downarrow$ polarization states, respectively. This result shows that the heterostructure is energetically stable under a vdW interlayer interaction.

Then, we discuss the electronic properties of VSi_2N_4 manipulated by the polarization of Sc_2CO_2 . In comparison with the band structure of freestanding VSi_2N_4 (Fig. 1(b)), there is an obvious upshift of E_F of VSi_2N_4 in the heterostructure with Sc_2CO_2 in the $\text{P}\uparrow$ polarization (Figs. 2(a) and 2(b)). As a result, a half-semiconductor to half-metal transition occurs in VSi_2N_4 . Moreover, the band gap of spin-up electrons remarkably decreases from 0.7 eV to 0.1 eV, showing the strong interface effect on the electronic structure of VSi_2N_4 . It is noticed that the spin-up energy bands in the heterostructure present a type-III band alignment, whereas the spin-down energy bands have a type-II band alignment. This feature indicates that there is an obvious electron transfer from Sc_2CO_2 to VSi_2N_4 , which fills up the spin-up conduction states. As for the case Sc_2CO_2 in $\text{P}\downarrow$ polarization, the spin-up energy bands of VSi_2N_4 present a type-I band alignment, and the spin-down energy bands form a type-II band alignment (Figs. 2(c) and 2(d)). This result shows that there is little charge transfer between Sc_2CO_2 and VSi_2N_4 . Compared to that of freestanding VSi_2N_4 , there is also a sizable decrease of band gap of the spin-up electrons (from 0.7 eV to 0.2 eV), whereas the band gap of spin-down electrons changes little. This result is similar to that of Sc_2CO_2 in $\text{P}\uparrow$ polarization. It is noticed that the E_F lies in the band gap of spin-up electrons, which makes the heterostructure a half-semiconductor. The above results show that the inversion of out-of-plane polarization of Sc_2CO_2 can dramatically change the band alignment as well as the band structure of VSi_2N_4 in the heterostructure.

To further show the Sc_2CO_2 -polarization dependent charge transfer effect on band structure of VSi_2N_4 ,

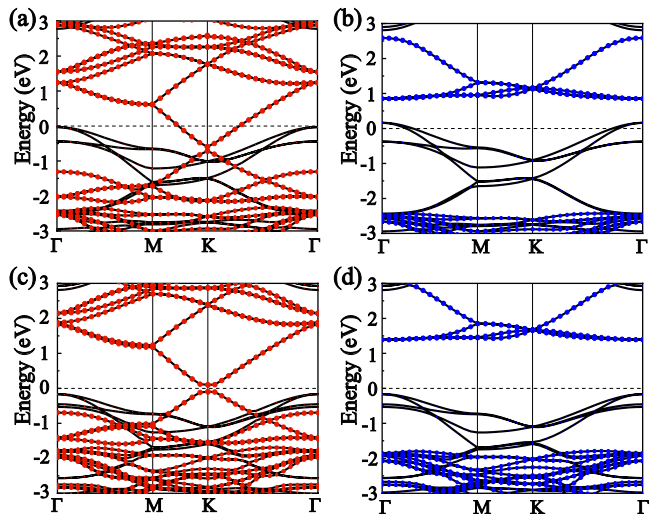


FIG. 2. Spin-resolved energy bands of $\text{VSi}_2\text{N}_4/\text{Sc}_2\text{CO}_2$ heterostructure with Sc_2CO_2 in $\text{P}\uparrow$ (a,b) and $\text{P}\downarrow$ (c,d) polarizations. (a) and (c) are the energy bands of spin-up electrons, (b) and (d) are the energy bands of spin-down electrons. Red and blue symbols denote spin-up and spin-down electronic states of VSi_2N_4 , respectively.

we calculate the electron density difference (EDF) of $\text{VSi}_2\text{N}_4/\text{Sc}_2\text{CO}_2$ heterostructure. As shown in Fig. 3(a), in comparison with that of freestanding VSi_2N_4 (Sc_2CO_2), there are extra electrons (holes) in the VSi_2N_4 (Sc_2CO_2) part in the $\text{P}\uparrow$ state. According to Bader's charge analysis, around 0.26 e transfers from Sc_2CO_2 to VSi_2N_4 , resulting in a half-semiconductor to half-metal transition of VSi_2N_4 . On the other hand, the charge transfer from Sc_2CO_2 to VSi_2N_4 in the $\text{P}\downarrow$ state is much smaller (0.03 e, see Fig. 3(b)). Hence, VSi_2N_4 holds a half-semiconductor characteristic. This result agrees well with the Sc_2CO_2 -polarization dependent band alignments in the heterostructure.

To understand the origin of charge transfer from Sc_2CO_2 to VSi_2N_4 , we have additionally explored the band alignment between freestanding Sc_2CO_2 and freestanding VSi_2N_4 . As shown in Fig. S2, type-I band alignment is obtained when Sc_2CO_2 is in either $\text{P}\uparrow$ or $\text{P}\downarrow$ polarizations. This result indicates little charge transfer occurs between Sc_2CO_2 and VSi_2N_4 from the viewpoint of relative electrostatic potential. Nonetheless, there is another mechanism for the interfacial charge transfer, i.e., electronegativity difference between elements^{30,31}. In the $\text{VSi}_2\text{N}_4/\text{Sc}_2\text{CO}_2$ heterostructure, charge transfer at the interface mainly occurs between N atoms of VSi_2N_4 (in the bottom layer) and Sc atoms of Sc_2CO_2 (in the top layer), owing to the large atomic radius (Sc) and short inter-atomic distances. Since the electronegativity of N and Sc are 3.04 and 1.36, respectively, electrons prefer to transfer from Sc to N, resulting in the charge transfer from Sc_2CO_2 to VSi_2N_4 . Note that the smaller charge transfer from Sc_2CO_2 to VSi_2N_4 in the $\text{P}\downarrow$ state can be

attributed to the larger interlayer distance.

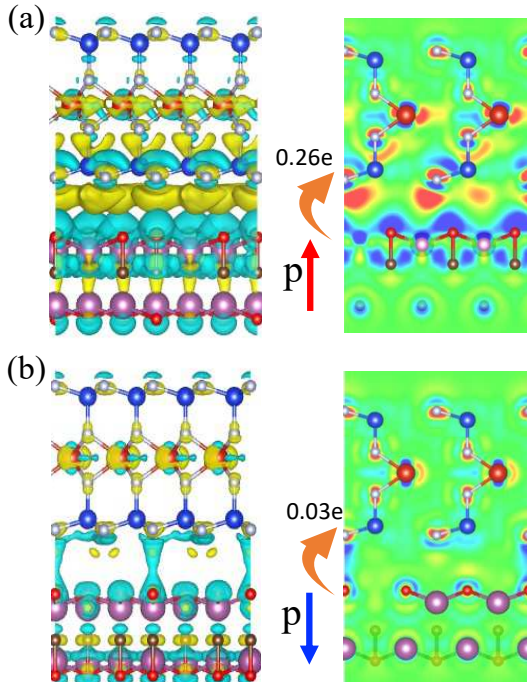


FIG. 3. Electron density difference (EDF) of $\text{VSi}_2\text{N}_4/\text{Sc}_2\text{CO}_2$ heterostructure. (a) EDF with Sc_2CO_2 in $P\uparrow$ polarization. (b) EDF with Sc_2CO_2 in $P\downarrow$ polarization. The left panels in (a) and (b) are the isosurface of EDF, where the yellow and azure colors represent the positive and negative values, respectively. The right panels in (a) and (b) are the contour plots of EDF, where the red and blue colors correspond to the normalized maximum of the positive and negative values, respectively.

In addition, the band projection analysis (Fig. S3) shows that both the conduction band minimum (CBM) and valence band maximum (VBM) of spin-up electronic states of VSi_2N_4 are attributed to the d_{z^2} and $d_{x^2-y^2}$ (e_g orbitals of V atoms), which located in the center of VSi_2N_4 . Note that the e_g orbitals of V atoms also give rise to the CBM of spin-down electrons as shown in Fig. S3, and thus induce the type-II band alignment. This result shows that the atomic layer composed of V atoms is mainly in charge of the spin current in the $\text{VSi}_2\text{N}_4/\text{Sc}_2\text{CO}_2$ heterostructure.

It is noticed that in both $P\uparrow$ and $P\downarrow$ states, V atoms of VSi_2N_4 gain sizable electrons in the heterostructure (Fig. 3). Since both CBM and VBM are mainly attributed to d orbitals of V, the band gap is particularly sensitive to the electron doping around V atoms, which leads to considerable reduction of band gap. To confirm such an argument, we have additionally calculated the band structure of monolayer VSi_2N_4 by electron doping. As shown in Fig. S4, the band gap of VSi_2N_4 remarkably decreases from 0.7 eV to 0.1 eV with 0.5 e doping in the simulated cell. It is noteworthy that VSi_2N_4 also transforms from a half-semiconductor to a half-metal due to

the downshift of CBM, when the doped electron is sizable.

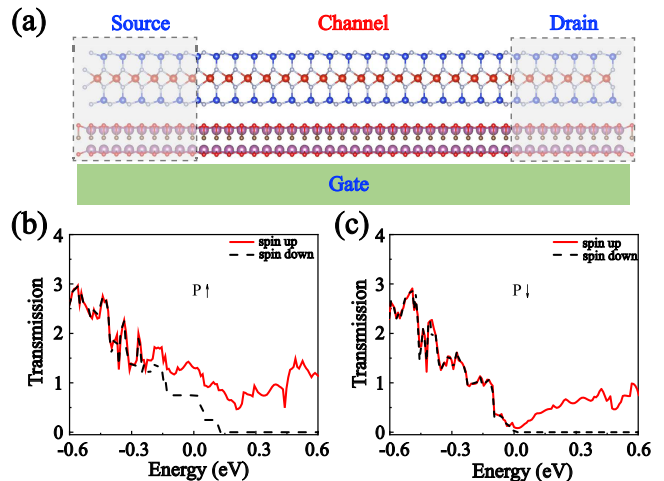


FIG. 4. (a) The schematic structure of the proposed Spin-FET based on the $\text{VSi}_2\text{N}_4/\text{Sc}_2\text{CO}_2$ heterostructure. (b) The calculated spin-polarized transmission spectrum of the Spin-FET with Sc_2CO_2 in $P\uparrow$ polarization. (c) The calculated spin-polarized transmission spectrum of the Spin-FET with Sc_2CO_2 in $P\downarrow$ polarization.

Next, we discuss the plentiful nonvolatile spin transport properties of VSi_2N_4 induced by the Sc_2CO_2 polarizations. We first propose a novel Spin-FET structure based on the $\text{VSi}_2\text{N}_4/\text{Sc}_2\text{CO}_2$ heterostructure, as shown in Fig. 4(a). In this structure, one can effectively control the inversion of Sc_2CO_2 ferroelectric polarization by a bottom gate. When Sc_2CO_2 is in $P\uparrow$ polarization, according to the band structure of $\text{VSi}_2\text{N}_4/\text{Sc}_2\text{CO}_2$ shown in Fig. 2(a), one expects a large spin-up current and thus the Spin-FET is in an *on* state, due to the half-metal characteristic of VSi_2N_4 . In contrast, when Sc_2CO_2 is in $P\downarrow$ polarization, a small spin-up current and thus the *off* state is expected within a low bias voltage region, owing to the half-semiconductor characteristic of VSi_2N_4 (Figs. 2(c)). Note that, there is no spin-down current from VSi_2N_4 , due to the large band gap of the spin-down electrons of VSi_2N_4 (Figs. 2(b) and 2(d)). Consequently, a pure spin-polarized current can be realized in the $\text{VSi}_2\text{N}_4/\text{Sc}_2\text{CO}_2$ based nonvolatile Spin-FET.

To verify above argument, we have also calculated the electronic transport property of the Spin-FET. Figs. 4(b) and 4(c) show the transmission spectrum of this device at zero bias with Sc_2CO_2 in $P\uparrow$ and $P\downarrow$ polarizations, respectively. It is seen that the transmission of spin-up electrons in $P\uparrow$ state reaches up to 1.4 at the Fermi level, whereas it is only 0.1 in the $P\downarrow$ state. The nonzero transmission at Fermi level in the $P\downarrow$ state can be attributed to the nonzero broadening parameter in the Green's function approach. As a result, an on-off ratio of 14 for the spin-up electrons of VSi_2N_4 can be obtained in the low bias voltage region. Notably, in the $P\uparrow$ state, there is also

sizable transmission at Fermi level (0.7) for the spin-down electrons, which comes entirely from Sc_2CO_2 (as shown in Fig. 2(b), the VBM of spin-down electrons of Sc_2CO_2 upshifts to 0.2 eV above E_F). This result shows an interesting spatially-separated spin-polarized transport phenomenon in the Spin-FET, which has potential applications in the future spintronics. Note that the transmission of spin-down electrons of both VSi_2N_4 and Sc_2CO_2 in the Spin-FET goes to zero at higher energy levels, i.e., $E \geq 0.15$ eV and 0.01 eV with Sc_2CO_2 in $P\uparrow$ and $P\downarrow$ states, respectively. In this condition, the spin-down current from Sc_2CO_2 can be completely inhibited, and thus the pure spin-up current can be realized. This result implies the good spin-valve performance of the $\text{VSi}_2\text{N}_4/\text{Sc}_2\text{CO}_2$ based devices. In addition, a more distinct transporting difference between the half-metal VSi_2N_4 in the heterostructure and the intrinsic VSi_2N_4 is expected owing to its larger intrinsic band gap (0.7 eV).

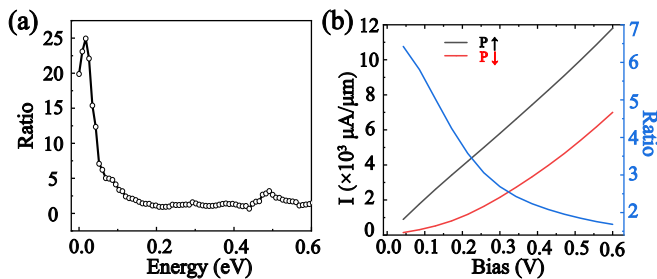


FIG. 5. (a) The ratio of total transmission (sum of spin-up and spin-down transmission) between the $P\uparrow$ and $P\downarrow$ polarization states. (b) The calculated I-V curves of the total current (sum of spin-up and spin-down current) with Sc_2CO_2 in $P\uparrow$ (solid red line) and $P\downarrow$ (solid black line) polarizations, respectively. The blue line in (b) shows the on-off ratio of total current.

Then we come to discuss the on-off ratio of the total current in the Spin-FET. Fig. 5(a) shows the on-off ratio of the total transmission (sum of spin-up and spin-down transmissions). It is seen that the on-off ratio monotonically increases with decreasing the bias voltage from 0.6 V, reaching 2500% around the Fermi level. This result indicates that a drastic total current (sum of spin-up and spin-down currents) difference can be induced by the inversion of ferroelectric polarizations of Sc_2CO_2 in the low bias voltage region. Fig. 5(b) further shows the calculated I-V curves of the total current in $P\uparrow$ and $P\downarrow$ states, respectively. In the $P\uparrow$ state, the total current linearly increases with the bias voltage. Whereas, in the $P\downarrow$ state it quadratically increases with the bias voltage. As a result, the on-off ratio of total current monotonically increases with decreasing the voltage, and a large on-off ratio of about 650% can be obtained when a small bias voltage (0.02 V) is applied (Fig. 5(b)).

Finally, we discuss the channel length of the $\text{VSi}_2\text{N}_4/\text{Sc}_2\text{CO}_2$ based spin-FETs. The channel length can be estimated by the spin diffusion length (λ), which is in-

versely proportional to the spin-orbit coupling (SOC) strength of channel materials. Unfortunately, there is no report on λ of VSi_2N_4 so far. Since N and Si are the light elements in periods 2 and 3, respectively, both of their SOC strength are very weak, contributing to a large λ . Indeed, it has been found that the bulk Si has a large λ of 2-3 μm ³². On the other hand, V is a transition metal in period 4, which would be responsible for the lower limit of λ in VSi_2N_4 . It has been found that pure V films has a spin diffusion length of about 15 nm due to the strong d-orbital based SOC³³. Considering that the d-orbital density of states in VSi_2N_4 is much smaller than that in V films, one can expect a larger λ in VSi_2N_4 , which might be tens of nanometers. Consequently, a channel length about tens of nanometers is expected in the $\text{VSi}_2\text{N}_4/\text{Sc}_2\text{CO}_2$ Spin-FETs.

IV. SUMMARY

In summary, based on the $\text{VSi}_2\text{N}_4/\text{Sc}_2\text{CO}_2$ multiferroic heterostructure, we propose a way of realizing nonvolatile Spin-FET, which has a low-energy-consumption characteristic. The DFT calculations show that the inversion of Sc_2CO_2 ferroelectric polarization can efficiently modulate the spin-polarized electronic structure of VSi_2N_4 , which induces a half-semiconductor to half-metal transition. Such electronic phase transition can lead to significant change of electronic transport properties, which is an essential concept of the nonvolatile Spin-FET. We additionally construct a Spin-FET device based on the $\text{VSi}_2\text{N}_4/\text{Sc}_2\text{CO}_2$ heterostructure. The electronic transport calculations show that the Spin-FET has remarkable all-electric-controlled performance, where a large on-off ratio (about 650%) of the total current has been obtained when a small bias voltage (0.02 V) is applied. Moreover, an interesting spatially-separated spin-polarized transport phenomenon has been observed when Sc_2CO_2 is in $P\uparrow$ polarization, with a pure spin-up (spin-down) current in VSi_2N_4 (Sc_2CO_2), respectively. These findings can be helpful to the design of high-performance nonvolatile 2D Spin-FET devices.

Before closing, we remark that continuously reducing the bias voltage is in line with the requirement of International Roadmap of Semiconductors (ITRS)³⁴, which benefits to the low-power chips. Although there has been no specific roadmap for the spintronic chip by far, one can expect a smaller bias to be utilized in spintronic devices due to its low-power nature, which makes the small working bias of $\text{VSi}_2\text{N}_4/\text{Sc}_2\text{CO}_2$ based Spin-FET possible. Moreover, a larger bias voltage can be achieved by properly selecting the composite of 2D multiferroic heterostructures, which is to be explored in the future works.

ACKNOWLEDGMENTS

We acknowledge financial support from the Ministry of Science and Technology of the People's Republic of China (Grant No. 2022YFA1402901), Science Fund for Distinguished Young Scholars of Shaanxi Province

(No. 2024JC-JCQN-09), the Natural Science Foundation of Shaanxi Province (Grant No. 2023-JC-QN-0768), the Natural Science Foundation of China (Grant No. 12074301), and Science and technology plan of Xi'an (Nos.2021XDJH05, 202211080023).

-
- * zxguo08@xjtu.edu.cn
- ¹ Z. Shen, S. Jing, Y. Heng, Y. Yao, K. N. Tu, and Y. Liu, *Appl. Phys. Rev.* **10**, 021309 (2023).
 - ² H. Li, H. Jiang, Q. F. Sun, and X. C. Xie, [arXiv:2303.07692](https://arxiv.org/abs/2303.07692).
 - ³ S. A. Wolf, A. Y. Chtchelkanova, and D. M. Treger, *IBM J. Res. Dev.* **50**, 101 (2006).
 - ⁴ A. Avsar, H. Ochoa, F. Guinea, B. Özyilmaz, B. J. van Wees, and I. J. Vera-Marun, *Rev. Mod. Phys.* **92**, 021003 (2020).
 - ⁵ A. Zhang, Z. Gong, Z. Zhu, A. Pan, and M. Chen, *Phys. Rev. B* **102**, 155413 (2020).
 - ⁶ M. Chen and F. Liu, *Natl. Sci. Rev.* **8**, nwaa241 (2021).
 - ⁷ H. Zhang, Y. Wang, W. Yang, J. Zhang, X. Xu, and F. Liu, *Nano Lett.* **21**, 5823 (2021).
 - ⁸ H. Zhang, W. Yang, P. Cui, X. Xu, and Z. Zhang, *Phys. Rev. B* **102**, 115413 (2020).
 - ⁹ S. Sugahara and J. Nitta, Spin-transistor electronics: An overview and outlook, *Proc. IEEE* **98**, 2124 (2010).
 - ¹⁰ S. Datta and B. Das, Electronic analog of the electrooptic modulator, *Appl. Phys. Lett.* **56**, 665 (1990).
 - ¹¹ B. Behin-Aein, D. Datta, S. Salahuddin, and S. Datta, *Nat. Nanotechnol.* **5**, 266 (2010).
 - ¹² B. Dieny, I. L. Prejbeanu, K. Garello, P. Gambardella, P. Freitas, R. Lehdorff, W. Raberg, U. Ebels, S. O. Demokritov, J. Akerman et al., *Nat. Nanotechnol.* **3**, 446 (2020).
 - ¹³ G. F. A. Malik, M. A. Kharadi, F. A. Khanday, and N. Parveen, *Microelectron. J.* **106**, 104924 (2020).
 - ¹⁴ L. Wang, Y. Shi, M. Liu, A. Zhang, Y. L. Hong, R. Li, Q. Gao, M. Chen, W. Ren, H. M. Cheng et al., *Nat. Commun.* **12**, 2361 (2021).
 - ¹⁵ M. Rakibul Karim Akanda and R. K. Lake, *Appl. Phys. Lett.* **119**, 052402 (2021).
 - ¹⁶ L. Liang, Y. Yang, X. Wang, and X. Li, *Nano Lett.* **23**, 858 (2023).
 - ¹⁷ Y. Lu, R. Fei, X. Lu, L. Zhu, L. Wang, and L. Yang, *ACS Appl. Mater. Interfaces* **12**, 6243 (2020).
 - ¹⁸ L. Cao, X. Deng, G. Zhou, S. J. Liang, C. V. Nguyen, L. K. Ang, and Y. S. Ang, *Phys. Rev. B* **105**, 165302 (2022).
 - ¹⁹ Y. Wang, X. Xu, W. Ji, S. Li, Y. Li, and X. Zhao, *Npj Comput. Mater.* **9**, 223 (2023).
 - ²⁰ X. Yu, X. Zhang, and J. Wang, *ACS Nano* **17**, 25348 (2023).
 - ²¹ J. Yang, B. Wu, J. Zhou, J. Lu, J. Yang, and L. Shen, *Nanoscale* **15**, 16103 (2023).
 - ²² J. Ding, D. F. Shao, M. Li, L. W. Wen, and E. Y. Tsymbal, *Nano Lett.* **21**, 175 (2021).
 - ²³ G. Kresse and J. Furthmüller, *Phys. Rev. B* **54**, 11169 (1996).
 - ²⁴ G. Kresse and J. Hafner, *Phys. Rev. B* **47**, 558 (1993).
 - ²⁵ K. Wang, Y. Zhang, W. Zhao, P. Li, J. W. Ding, G. F. Xie, and Z. X. Guo, *Phys. Chem. Chem. Phys.* **21**, 9310 (2019).
 - ²⁶ Z. X. Guo, Y. Y. Zhang, H. J. Xiang, X. G. Gong, and A. Oshiyama, *Phys. Rev. B* **92**, 201413(R) (2015).
 - ²⁷ S. Smidstrup, T. Markussen, P. Vancaeyveld, J. Wellendorff, J. Schneider, T. Gunst, B. Verstichel, D. Stradi, P. A. Khomyakov, U. G. Vej-Hansen et al., *J. Phys.: Condens. Matter* **32**, 015901 (2020).
 - ²⁸ J. Huang, P. Li, X. Ren, and Z. X. Guo, *Phys. Rev. Appl.* **16**, 044022 (2021).
 - ²⁹ B. Liu, X. X. Ren, X. Zhang, P. Li, Y. Dong, Z. X. Guo, *Appl. Phys. Lett.* **122**, 152408 (2023).
 - ³⁰ H. Chen, H. Park, A. J. Millis, and C. A. Marianetti, *Phys. Rev. B* **90**, 245138 (2014).
 - ³¹ P. Li, X. S. Zhou, and Z. X. Guo, *Npj Comput. Mater.* **8**, 20 (2022).
 - ³² T. Sasaki, T. Oikawa, T. Suzuki, M. Shiraishi, Y. Suzuki, and K. Noguchi, *Appl. Phys. Lett.* **96**, 122101 (2010).
 - ³³ C. Du, H. Wang, F. Yang, and P. C. Hammel, *Phys. Rev. B* **90**, 140407(R) (2014).
 - ³⁴ B. Hoefflinger, *CHIPS* **2**, 143 (2020).